Identification of open loop dynamics of a manual controlled bicycle-rider system

Jason K. Moore and Mont Hubbard

September 30, 2013

Introduction

Today's experiments are capable of delivering a staggering amount of both kinematic and kinetic data from complex dynamical systems. Such a large amount of data lends itself to data driven modeling approaches that can potentially provide more predictive models than first principles models. These data driven models can also give insight into the deficiencies of first principles models. Here we explore the bicycle-rider system with data driven modeling.

The bicycle/motorcycle-rider system has been described with a variety of models. Many studies of bicycles rely on the benchmarked Whipple model [9], with or without the addition of tire models, for analytical studies of the system and simulation comparisons. The Whipple bicycle model [13] is regarded as a highly predictive, yet "simple", model of the bicycle-rider system and is constructed from first principles, yet very little experimental data proves it robustly predicts bicycle-rider open loop dynamics.

We are aware of only three significant attempts to validate the Whipple bicycle model with experimental data. The most cited [7, 6] show that the Whipple model is predictive of a *riderless* bicycle in a gymnasium and on a treadmill for speeds in its predicted stable speed range, 4-6 m/s. The other [1] shows that the Whipple model linearized in a steady turn predicts kinematics but not the rider's applied steering torque. Open loop motorcycle-rider system dynamics have been identified [3] and [4, 5]. Eaton used frequency domain identification techniques, known to be problematic for closed loop identification [8]. James showed that identified ARX models with lower order than typical first principles models can predict the measured motion, but did not find very good agreement with his high order first principles models.

We have collected a large set of time history data from an instrumented bicycle under manual control. The measurements include the most important kinematic and kinetic variables describing bicycle-rider motion from three riders on the same bicycle for a variety of maneuvers and speeds. These experiments generated approximately 1.7 million time samples from about 30 sensors sampled at 200 hertz (about 2.4 hours of real time).

There is good reason to question some of assumptions in the Whipple model, namely knife-edge no-slip wheels, especially under full rider weight. In addition, rider biomechanics have a larger influence on and coupling to the bicycle than the motorcycle. Our identified models attempt to account for these and other discrepancies.

Instrumented Bicycle Experiments

We instrumented a bicycle with a unique combination of dynamic sensors. Rider biomechanical movement, including pedaling, was restricted to make the Whipple rigid-rider assumption more applicable and the bicycle was propelled by an electric motor, Figure . Experiments were performed both on the open road and on a treadmill. Rear frame 3D angular rates and a 3D point acceleration were measured with a VectorNav VN-100 inertial measurement unit; rear frame roll angle with a rotary potentiometer on a lightweight trailer; steer angle using a rotary potentiometer; axial

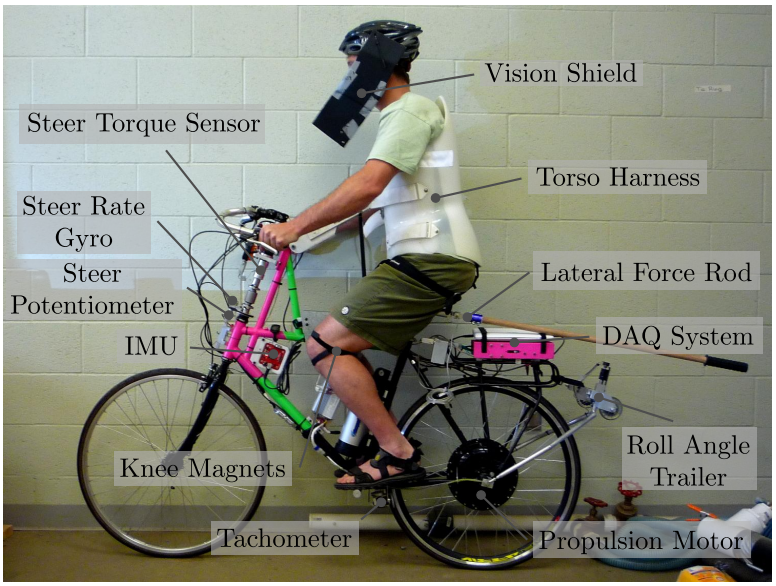

Figure 1: The instrumented bicycle with rider L seated in the harness.

Table 1: The fundamental measurements from the instrumented bicycle.

Variable	Description	Units
v	wheel center speed magnitude	m/s
δ, ϕ, ψ	steer, roll and yaw angles	rad
$\dot{\delta}, \dot{\phi}, \dot{\psi}, \dot{\theta}_B$	steer, roll, yaw, and rear wheel angular rates	rad/s
T_δ, F	steer torque, lateral perturbation force	NM, N

torque in the steer tube with a Futek 150 in-lb (17 Nm) TFF350 torque sensor; lateral seat-post perturbation force by a 100 lb load cell (Interface SSM-100); inertial angular rate of the front frame about the steer axis by a single axis rate gyro (Silicon Sensing CRS03-04S); and rear wheel angular rate by a DC generator, Figure . See [11] for full details of the equipment.

The analysis herein focuses on two maneuvers we call *Heading Tracking* and *Lateral Deviation Tracking*. During heading tracking the rider was instructed simply to balance the bicycle and keep a relatively constant heading while focusing their vision at a point in the distance. During lateral deviation tracking the rider focused on a straight line marked on the ground and attempted to keep the front wheel on this line. Both tasks were performed with and without manually applied lateral perturbation forces just below the seat, random in direction and time during the trials. Each maneuver was performed on both a 1 meter wide treadmill and an open gymnasium floor [11].

Physical parameters (geometry, mass, center of mass, and moments of inertia) of both bicycle and rider were estimated using the methods in [11] and [14]. Bicycle geometry was measured to get accurate estimates of the parameters used in the benchmark model, [9]. Combined inertial properties of the bicycle rear frame and rider were computed with standard methods. Two open source software packages, `yeadon` [2] and `BicycleParameters` [10] manage and process the physical parameter data.

Before each day of testing, base data were collected for the system's sensors for calibration purposes. Then for each trial a set of meta data and raw time series were collected from the bicycle's on-board DAQ system. This data was stored in a HDF5 database for easy querying and retrieval in the data analysis step. Raw data was then processed to obtain the desired time histories defined by the Whipple model coordinates, described in Table 1.

Signals were measured and processed as described in [11]. Roll and steer accelerations were estimated by numerically differentiating roll and steer rate signals. Before identification computations we subtracted the temporal means of the signals that were generally symmetric about zero, i.e. all but lateral force and speed. Then all signals were filtered with a second order low pass Butterworth filter at a 15 Hz cutoff frequency. Experimental data was collected over seven days and comprised about 600 individual trials with three riders. We used 374 of the runs for the following analysis.

Identification

The linear Whipple model is a 4th order system with roll angle ϕ, steer angle δ, roll rate $\dot{\phi}$, and steer rate $\dot{\delta}$ selected as the independent states and with roll T_ϕ and steer T_δ torques as the generalized forces and system inputs. In place of the roll torque input, we extend the model to include a lateral force F acting at a point on the frame to provide a new input, accurately modelling imposed lateral perturbations [11]. We also examine a second candidate model which adds the inertial effects of the rider's arms to the Whipple model, also described in [11]. This model was designed to more accurately account for the fact that the riders were free to move their arms with the front frame of the bicycle. This model is similar to the upright rider in [12], but with slightly different joint definitions. Constraints are chosen so that no additional degrees of freedom are added, keeping the system both tractable and comparable to the benchmarked Whipple model.

We make the assumptions that the model is linear and fourth order, and that we can measure the states and inputs directly while the system is under rider closed loop control. We then employ the *direct identification* approach to identify the plant [8].

Identification of the bicycle-rider equations of motion can be formulated with respect to an augmented benchmark canonical form based on [9],and shown in Equation 1. If the time varying quantities in the equations are all measured at each time step, the coefficients of the linear equations can be estimated, given enough time steps.

$$\mathbf{M}\ddot{q} + v\mathbf{C}_1\dot{q} + [g\mathbf{K}_0 + v^2\mathbf{K}_2]q = T + HF \tag{1}$$

where the time-varying states roll and steer are collected in the vector $q = [\phi \quad \delta]^T$, the time varying roll torque and steer torque inputs are collected in the vector $T = [T_\phi \quad T_\delta]^T$, and $H = [H_{\phi F} \quad H_{\delta F}]^T$ is a coefficient vector describing the linear contribution of the lateral force, F, to the roll and steer torque equations. This equation assumes speed, v, is constant since the model was linearized about a constant speed equilibrium. We treat v as a time varying parameter because the measured longitudinal acceleration is negligible.

A simple analytic identification problem can be formulated from the canonical form. If we have good measurements of q, their first and second derivatives, forward speed v, and the inputs T_δ and F, the entries in $\mathbf{M}$, $\mathbf{C}_1$, $\mathbf{K}_0$, $\mathbf{K}_2$, and H can be identified by forming two simple linear regressions (one for each equation in the canonical form).

The roll and steer equations each can be put into a simple linear form:

$$\mathbf{\Gamma}\Theta = Y \tag{2}$$

where Θ is a vector of the unknown constant matrix entries and the design matrix $\mathbf{\Gamma}$ and prediction vector Y are made up of inputs and outputs measured during a run. Θ can be all or a subset of the entries in the canonical matrices and can be estimated using the well known linear least squares solution.

$$\hat{\Theta} = [\mathbf{\Gamma}^T\mathbf{\Gamma}]^{-1}\mathbf{\Gamma}^T Y \tag{3}$$

Equation 3 can be solved for each run individually, a portion of a run, or a set of runs.Also, all of the parameters in the canonical matrices need not be estimated. The analytical formulation of the Whipple model bicycle model [9] gives a good idea of which entries in the matrices we may be

more certain about from our physical parameters measurements. We fixed any parameters which were not a function of trail, front assembly moments and products of inertia, or equal to zero. This is because the true trail is difficult to measure, and the inertia of the front frame plays a large roll in the steer dynamics.

For the roll equation this leaves $M_{\phi\delta}$, $C_{1\phi\delta}$, and $K_{0\phi\delta}$ as free parameters, and for the steer equation this leaves $M_{\delta\phi}$, $M_{\delta\delta}$, $C_{1\delta\phi}$, $C_{1\delta\delta}$, $K_{0\delta\phi}$, $K_{0\delta\delta}$, $K_{2\delta\delta}$, and $H_{\delta F}$ as free parameters.

We start by identifying the three coefficients of the roll equation for the given data using

$$\begin{bmatrix} \ddot{\delta}(1) & v(1)\dot{\delta}(1) & g\delta(1) \\ \vdots & \vdots & \vdots \\ \ddot{\delta}(N) & v(N)\dot{\delta}(N) & g\delta(N) \end{bmatrix} \begin{bmatrix} M_{\phi\delta} \\ C_{1\phi\delta} \\ K_{0\phi\delta} \end{bmatrix} \tag{4}$$
$$= \begin{bmatrix} H_{\phi F}F(1) - M_{\phi\phi}\ddot{\phi}(1) - C_{1\phi\phi}v(1)\dot{\phi}(1) - K_{0\phi\phi}g\phi(1) - K_{2\phi\phi}v(1)^2\phi(1) - K_{2\phi\delta}v(1)^2\delta(1) \\ \vdots \\ H_{\phi F}F(N) - M_{\phi\phi}\ddot{\phi}(N) - C_{N\phi\phi}v(N)\dot{\phi}(N) - K_{0\phi\phi}g\phi(N) - K_{2\phi\phi}v(N)^2\phi(N) - K_{2\phi\delta}v(N)^2\delta(N) \end{bmatrix}$$

We then enforce the assumptions that $M_{\phi\delta} = M_{\delta\phi}$ and $K_{0\phi\delta} = K_{0\delta\phi}$ to fix these values in the steer equation to the ones identified in the roll equation, leaving fewer free parameters in the steer equation. Finally, we identify the remaining steer equation coefficients with

$$\begin{bmatrix} \ddot{\delta}(1) & v(1)\dot{\phi}(1) & v(1)\dot{\delta}(1) & g\phi(1) & v(1)^2\delta(1) & -F(1) \\ \vdots & \vdots & \vdots & \vdots & \vdots & \vdots \\ \ddot{\delta}(N) & v(N)\dot{\phi}(N) & v(N)\dot{\delta}(N) & g\phi(N) & v(N)^2\delta(N) & -F(N) \end{bmatrix} \begin{bmatrix} M_{\delta\delta} \\ C_{1\delta\phi} \\ C_{1\delta\delta} \\ K_{0\delta\phi} \\ K_{2\delta\delta} \\ H_{\delta F} \end{bmatrix}$$
$$= \begin{bmatrix} T_\delta(1) - M_{\delta\phi}\ddot{\phi}(1) - K_{0\delta\delta}g\delta(1) - K_{2\delta\phi}v(1)^2\phi(1) \\ \vdots \\ T_\delta(N) - M_{\delta\phi}\ddot{\phi}(N) - K_{0\delta\delta}g\delta(N) - K_{2\delta\phi}v(N)^2\phi(N) \end{bmatrix} \tag{5}$$

Results

From our larger pool of data, we selected data for three riders on the same bicycle, performing two maneuvers, in two different environments. There is little reason to believe the dynamics of the open loop system should vary much with respect to different maneuvers, but there is potential variation across riders due to the differences in their inertial and musculoskeletal properties and there may be variation across environments because of the differences in the wheel-floor interaction. We computed the best fit model across a series of runs to benefit from the large dataset. We then selected four scenarios with a total of 12 different models: All riders in both environments [one data set], All riders in each environment [two data sets], Each rider in both environments [three data sets], Each rider in each environment [six data sets].

Model Quality

We used two methods to judge the quality of the identified models with respect to the available data: (1) we compute the variance accounted for (VAF, i.e. coefficent of determination) with respect to the linear least squares solution for each set of runs and each identified model and (2) we simulate the identified model given the measured steer torque and lateral force for each run and compute VAF with respect to the four predicted outputs and measured outputs.

The second method works well when the open loop system is stable, but if it is unstable as in the case of this bicycle, it may be difficult to simulate. Searching for initial conditions that give

Table 2: Roll equation VAF computed for each subset of data (rows) and each model (columns).

	A-A	A-H	A-P	C-A	C-H	C-P	J-A	J-H	J-P	L-A	L-H	L-P	Whipple
C-H	29.3%	29.6%	25.5%	30.5%	30.9%	29.6%	28.4%	28.2%	23.4%	27.8%	29.8%	18.1%	5.0%
C-P	18.3%	17.8%	17.6%	19.1%	18.6%	19.2%	17.6%	17.1%	16.4%	18.0%	17.8%	14.8%	8.7%
C-A	21.7%	21.4%	20.1%	22.7%	22.4%	22.5%	21.0%	20.5%	18.7%	21.1%	21.5%	15.9%	7.5%
J-H	30.5%	31.1%	27.0%	28.9%	29.5%	27.9%	30.8%	31.2%	26.1%	29.7%	30.3%	21.4%	-0.4%
J-P	47.6%	44.4%	50.0%	43.7%	43.0%	43.7%	47.6%	44.5%	50.5%	48.9%	41.3%	49.4%	36.1%
J-A	35.6%	35.1%	33.6%	33.4%	33.6%	32.6%	35.8%	35.3%	33.1%	35.3%	33.7%	29.3%	9.9%
L-H	25.5%	26.9%	20.1%	25.9%	26.5%	24.7%	25.1%	26.4%	18.2%	23.8%	27.4%	12.4%	-5.5%
L-P	47.2%	43.5%	51.6%	43.4%	41.8%	44.5%	47.2%	44.3%	52.2%	49.3%	40.2%	53.3%	48.5%
L-A	37.8%	36.5%	37.4%	36.0%	35.4%	36.0%	37.6%	36.6%	36.7%	38.1%	34.9%	34.2%	22.7%
A-H	29.6%	30.2%	25.7%	28.7%	29.3%	27.7%	29.5%	30.0%	24.4%	28.5%	29.8%	19.5%	2.8%
A-P	34.9%	33.0%	36.2%	33.4%	32.6%	33.7%	34.6%	32.8%	36.0%	35.7%	31.3%	35.0%	27.4%
A-A	32.1%	31.5%	30.5%	30.9%	30.8%	30.4%	31.9%	31.3%	29.6%	31.8%	30.5%	26.4%	13.6%

Table 3: Steer equation VAFcomputed for each subset of data (rows) and each model (columns).

	A-A	A-H	A-P	C-A	C-H	C-P	J-A	J-H	J-P	L-A	L-H	L-P	Whipple
C-H	58.3%	60.8%	49.4%	53.1%	59.1%	38.4%	60.8%	59.0%	56.8%	50.6%	53.5%	42.3%	61.4%
C-P	48.5%	50.7%	45.0%	44.4%	46.1%	39.8%	52.0%	51.3%	49.0%	41.8%	42.9%	38.3%	52.7%
C-A	52.9%	55.3%	47.1%	48.4%	51.9%	39.1%	56.0%	54.9%	52.6%	45.8%	47.7%	40.2%	56.7%
J-H	70.2%	69.9%	62.9%	66.0%	70.0%	50.2%	68.9%	66.8%	68.2%	66.2%	67.5%	58.5%	68.7%
J-P	72.3%	70.3%	71.6%	69.2%	65.6%	65.4%	71.0%	67.6%	73.5%	70.7%	68.5%	67.8%	68.1%
J-A	70.7%	70.0%	65.0%	66.8%	68.8%	53.8%	69.4%	67.0%	69.6%	67.4%	67.8%	60.7%	68.5%
L-H	67.8%	68.5%	58.7%	61.9%	67.2%	43.6%	67.6%	65.2%	66.4%	62.3%	63.7%	53.6%	67.0%
L-P	72.6%	70.6%	73.7%	68.9%	66.5%	62.9%	72.7%	68.3%	77.3%	68.9%	63.7%	69.1%	68.6%
L-A	70.1%	69.5%	65.3%	65.2%	66.8%	52.1%	70.0%	66.7%	71.2%	65.4%	63.7%	60.4%	67.7%
A-H	68.0%	68.4%	60.2%	63.4%	67.9%	47.4%	67.5%	65.4%	66.2%	63.2%	64.8%	55.2%	66.8%
A-P	64.8%	64.4%	63.5%	61.4%	60.0%	56.9%	65.6%	63.0%	66.4%	60.9%	59.3%	58.6%	63.1%
A-A	66.8%	66.9%	61.3%	62.7%	64.9%	50.6%	66.8%	64.5%	66.3%	62.4%	62.7%	56.4%	65.5%

rise to a stable model for the duration of the run or simulating by weighting the future error less may relieve the instability issues. We chose the former method for these computations.

For method (1) the *variance accounted for* (VAF) by the model for both the roll torque and the steer torque equations are

$$\text{VAF}_{\phi,\delta} = 1 - \frac{||\mathbf{\Gamma}_{\phi,\delta}\hat{\Theta}_{\phi,\delta} - Y_{\phi,\delta}||}{||Y_{\phi,\delta} - \bar{Y}_{\phi,\delta}||} \tag{6}$$

where $\bar{Y}$ is the mean of Y.

subsets scenario combinations models this is not clear We compute the two values of VAF for each of the subsets of data from the 12 scenario combinations using 13 models: the 12 identified models and the Whipple model. The columns in Tables 2 and 3 correspond to the models and the rows correspond to the data subsets the VAF was computed with. The maximum VAF in a row gives an indication of the best model for predicting that set of runs.

Tables 2 and 3 lead to these observations: the models predict steer torque better than roll torque, the Whipple model is generally poor at predicting roll torque, the Whipple model is good at predicting steer torque.

For method (2), we simulate all 14 models with the inputs measured from the 374 runs and compute the VAF explained by the model for each of the four outputs. Since the models are typically unstable at all of the speeds we tested, we searched for the set of initial conditions which minimizes the VAF for all outputs and ignored any runs in which suitable initial conditions couldn't be found. Table 4 presents the median percent variance accounted for across all runs for the outputs of each model. Based on the mean VAF across the outputs for each model the best model seems to be L-P. Notice that the Whipple model is the poorest predictor and the arm model is the second poorest.

The following are observed from Table 4: for all outputs other than roll angle, the arm model is better than the Whipple model; all of the identified models are better predictors than the first principles models; and model J-P has the best average predictive ability for all of the runs.

Most predictive model

This section details the characteristics for the identified model which best predicts *all* of the data, the L-P model.

Table 4: Median VAF, in percent, of each output variable over 374 runs for each model and their mean.

Model	ϕ	δ	$\dot{\phi}$	$\dot{\delta}$	Mean
A-A	28.6	61.8	51.8	65.2	51.8
C-H	18.6	57.2	52.6	62.2	47.7
L-A	29.4	59.8	52.9	67.9	52.5
A-H	24.1	57.4	43.1	64.2	47.2
C-A	14.9	54.5	51.7	59.8	45.2
J-P	-3.4	35.4	34.1	61.7	31.9
L-H	24.3	57.7	46.1	65.7	48.5
A-P	29.7	58.9	60.6	63.2	53.1
J-H	22.8	53.6	42.0	62.8	45.3
L-P	38.2	62.8	60.9	68.4	57.6
C-P	19.0	46.0	42.0	47.1	38.5
J-A	27.9	61.0	49.4	65.9	51.1
Whipple	-21.0	10.3	5.8	12.2	1.8
Arm	-33.1	19.6	29.7	33.1	12.3

Table 5: The identified $\mathbf{M}$, $\mathbf{C}_1$, $\mathbf{K}_0$, $\mathbf{K}_2$, and H matrices of the L-P and Whipple models.

Model	$\mathbf{M}$	$\mathbf{C}_1$	$\mathbf{K}_0$	$\mathbf{K}_2$	H
Whipple	$\begin{bmatrix} 129.362 & 2.260 \\ 2.260 & 0.219 \end{bmatrix}$	$\begin{bmatrix} 0.000 & 41.622 \\ -0.315 & 1.376 \end{bmatrix}$	$\begin{bmatrix} -115.707 & -2.361 \\ -2.361 & -0.737 \end{bmatrix}$	$\begin{bmatrix} 0.000 & 103.943 \\ 0.000 & 2.190 \end{bmatrix}$	$\begin{bmatrix} 0.902 \\ 0.011 \end{bmatrix}$
L-P	$\begin{bmatrix} 129.362 & 2.559 \\ 2.559 & 0.250 \end{bmatrix}$	$\begin{bmatrix} 0.000 & 33.526 \\ -0.549 & 2.100 \end{bmatrix}$	$\begin{bmatrix} -115.707 & -4.526 \\ -4.526 & -0.489 \end{bmatrix}$	$\begin{bmatrix} 0.000 & 103.943 \\ 0.000 & 2.603 \end{bmatrix}$	$\begin{bmatrix} 0.902 \\ 0.011 \end{bmatrix}$

The eigenvalues as a function of speed of the identified model can be compared to those of the Whipple and arm models. Figure 2 shows the root locus of the three models as a function of speed. The oscillatory weave mode exists in all three models, stable at all speeds in the arm model but unstable at lower speeds in the other two models. The identified model's oscillatory weave mode is unstable over most of the shown speed range. Above 3 m/s or so, the Whipple model's oscillatory weave mode diverges from the identified model to different asymptotes. The arm model weave mode diverges somewhere in between but shares similar pole locations with the Whipple model at higher speeds. Note that the arm model has an unstable real mode for all speeds.

Figure 3 gives a different view of the root locus allowing one to more easily compare the real and imaginary parts of the eigenvalues independently. The imaginary parts of the weave mode have similar curvature with respect to speed for all the models about 2m/s or so. The identified model has a stable speed range where the Whipple model under predicts its weave critical speed by almost 3 m/s. The identified caster mode is much faster than that predicted by the Whipple model. This is somewhat counterintuitive because tire scrub torques would probably tend to slow the caster mode, although the pneumatic trail and arm inertia could play larger roles than expected.

The frequency band from 1 rad/s to 12 rad/s is of most concern as it bounds a reasonable range that humans operate within. The steer torque to roll angle transfer function, Figure 4 may be the most important to model accurately as it is the primary method of controlling the bicycle's direction, i.e. commanding roll allows one to command yaw. At 2 m/s the magnitude is similar for all three models. At 4 m/s the identified model has a larger gain than the first principles models. In fact, the identified model seems to vary little with speed, which contrasts the stronger speed dependence of the first principles models. The low frequency behavior of the identified model is not well predicted by the Whipple and arm models at the three highest speeds but about about 3 rad/s the arm model shows better magnitude matches than the Whipple model.

Table gives the values of the identified coefficients of the roll and steer equations for the L-P model.

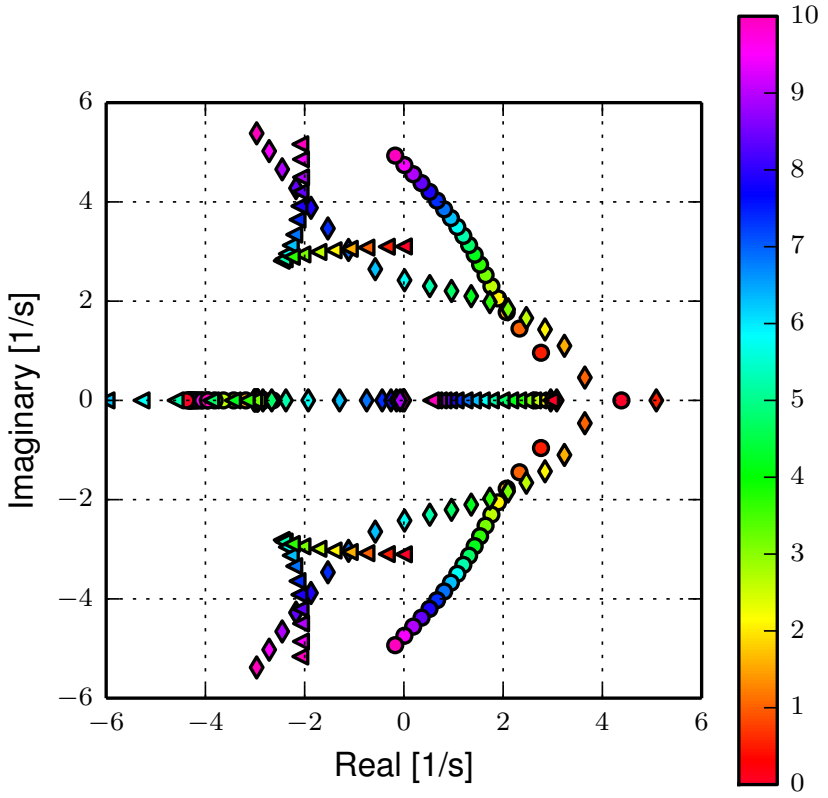

Figure 2: Root locus of the identified model (circle), the Whipple model (diamond), and the arm model (triangle) with respect to speed in m/s.

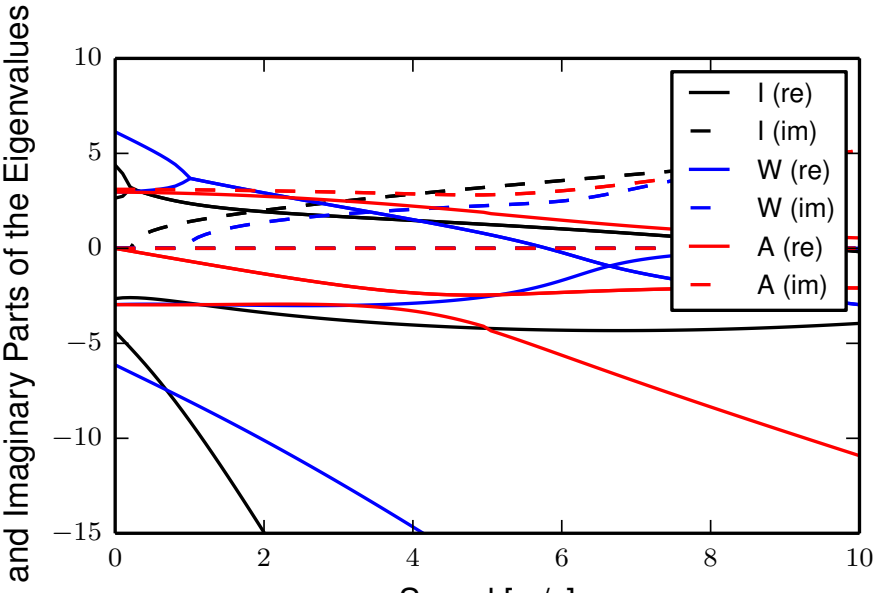

Figure 3: Real and imaginary parts of the eigenvalues as a function of speed for model (I)dentified from all runs, the (W)hipple model and the (A)rm model.

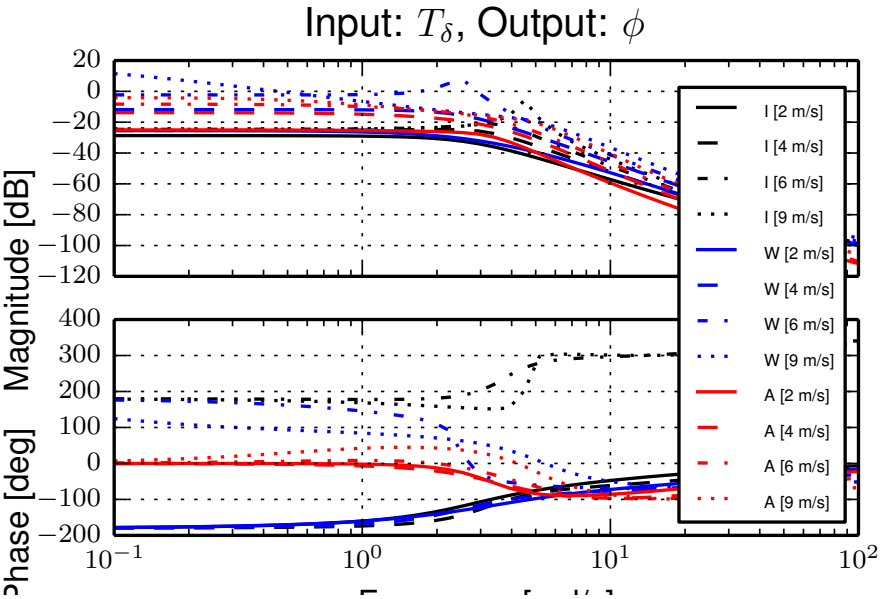

Figure 4: Frequency response of the three models, (I)dentified, (W)hipple, and (A)rm, at four speeds (2, 4, 6, and 9 m/s). The color indicates the model and the line type indicates the speed

Summary and Acknowledgements

We have shown that a fourth order linear model is adequate for describing the motion of the bicycle under manual control in a speed range from approximately 1.5 m/s to 9 m/s. Results from this study show that higher order models may not be necessary for predicting the bicycle-rider plant dynamics. This is an important finding, as many researchers develop models using first principles which have orders much greater than 4, with degrees of freedom associated with tire slip, frame flexibilities, and rider biomechanics, which may be overkill for many prediction purposes. But, results also reveal that fourth order archetypal first principles models are not predictive enough to fully describe the dynamics. These deficiencies are most likely due to un-modeled effects, with knife-edge, no side-slip wheel contact assumptions being the most probable candidate. Un-modeled rider biomechanics such as passive arm stiffness and damping and head motion may play a role too. It is likely that something as simple as a "static" tire scrub torque is needed to improve the fidelity of the Whipple first principles derivations, but that doesn't preclude that the addition of a tire slip model, adding more degrees of freedom, might also improve the predictive ability. This paper is based on work supported by the National Science Foundation under Grant No 0928339. Karl Åström provided the ideas for the canonical form.

References

[1] Stephen M. Cain and Noel C. Perkins. Comparison of experimental data to a model for bicycle steady-state turning. *Vehicle System Dynamics*, 50(8):1341–1364, 2012.

[2] Christopher Dembia. *Yeadon: A Python Library For Human Inertia Estimation*, 2011. http://pypi.python.org/pypi/yeadon/.

[3] David J. Eaton. *Man-Machine Dynamics in the Stabilization of Single-Track Vehicles*. PhD thesis, University of Michigan, 1973.

[4] Stephen R. James. Lateral dynamics of an offroad motorcycle by system identification. *Vehicle System Dynamics*, 38(1):1–22, July 2002.

[5] Stephen R James. Lateral dynamics of motorcycles towing single-wheeled trailers. *Vehicle System Dynamics: International Journal of Vehicle Mechanics and Mobility*, 43(8):581–599, 2005.

[6] J. D. G. Kooijman and A. L. Schwab. Experimental validation of the lateral dynamics of a bicycle on a treadmill. In *Proceedings of the ASME 2009 International Design Engineering Technical Conferences & Computers and Information in Engineering Conference, IDETC/CIE 2009*, number DETC2009-86965, 2009.

[7] J. D. G. Kooijman, A. L. Schwab, and J. P. Meijaard. Experimental validation of a model of an uncontrolled bicycle. *Multibody System Dynamics*, 19:115–132, May 2008.

[8] Lennart Ljung. *System Identification: Theory for the User*. Prentice Hall, second edition, 1999.

[9] J. P. Meijaard, Jim M. Papadopoulos, Andy Ruina, and A. L. Schwab. Linearized dynamics equations for the balance and steer of a bicycle: A benchmark and review. *Proceedings of the Royal Society A: Mathematical, Physical and Engineering Sciences*, 463(2084):1955–1982, August 2007.

[10] Jason K. Moore. *BicycleParameters: A Python library for bicycle parameter estimation and analysis*, 2011. http://pypi.python.org/pypi/BicycleParameters.

[11] Jason K. Moore. *Human Control of a Bicycle*. PhD thesis, University of California, Davis, Davis, CA, August 2012.

[12] A. L. Schwab and J. D. G. Kooijman. Lateral dynamics of a bicycle with passive rider model. In *The 1st Joint International Conference on Multibody System Dynamics*, Lappeenranta, Finland, May 2010.

[13] Francis J. W. Whipple. The stability of the motion of a bicycle. *Quarterly Journal of Pure and Applied Mathematics*, 30:312–348, 1899.

[14] M. R. Yeadon. The simulation of aerial movement–i. the determination of orientation angles from film data. *Journal of Biomechanics*, 23(1):59 – 66, 1990.